

See discussions, stats, and author profiles for this publication at: <https://www.researchgate.net/publication/343086797>

# Predicting evaporation from mountain streams

Article in *Hydrological Processes* · July 2020

DOI: 10.1002/hyp.13875

---

CITATIONS

3

---

READS

116

2 authors, including:



**Andras J Szeitz**

University of British Columbia - Vancouver

2 PUBLICATIONS 3 CITATIONS

SEE PROFILE



## Title Page

Title: Predicting evaporation from mountain streams

Running title: Predicting evaporation from mountain streams

Authors: Andras Janos Szeitz\*, Robert Daniel Moore

Institutional affiliations: Department of Geography, University of British Columbia, 1984 West Mall, Vancouver, BC, V6T 1Z4. Correspondence: aszeitz@gmail.com

Acknowledgements: This research was funded by a Natural Sciences and Engineering Research Council (NSERC) Discovery Grant to R D Moore, and an NSERC Canada Graduate Scholarship awarded to A J Szeitz. Anna Kaveney, Virgile Laurent and Johannes Exler assisted with field data collection and instrument calibration. J Leach and two anonymous reviewers provided constructive comments that helped us improve the manuscript.

This article has been accepted for publication and undergone full peer review but has not been through the copyediting, typesetting, pagination and proofreading process which may lead to differences between this version and the Version of Record. Please cite this article as doi: [10.1002/hyp.13875](https://doi.org/10.1002/hyp.13875)

## Predicting Evaporation from Mountain Streams

Abstract: Evaporation can be an important control on stream temperature, particularly in summer when it acts to limit daily maximum stream temperature. Evaporation from streams is usually modelled with the use of a wind function that includes empirically derived coefficients. A small number of studies derived wind functions for individual streams; the fitted parameters varied substantially among sites. In this study, stream evaporation and above-stream meteorological conditions (at 0.5 and 1.5 m above the water surface) were measured at nine mountain streams in southwestern British Columbia, Canada, covering a range of stream widths, temperatures, and riparian vegetation. Evaporation was measured on twenty site-days in total, at approximately hourly intervals, using nine floating evaporation pans distributed across the channels. The wind function was fit using mixed-effects models to account for among-stream variability in the parameters. The fixed-effects parameters were tested using leave-one-site-out cross-validation. The model based on 0.5-m measurements provided improved model performance compared to that based on 1.5-m values, with RMSE of 0.0162 and 0.0187 mm h<sup>-1</sup>, respectively, relative to a mean evaporation rate of 0.06 mm h<sup>-1</sup>. Inclusion of atmospheric stability and canopy openness as predictors improved model performance when using the 1.5-m meteorological measurements, with minimal improvement when based on 0.5-m measurements. Of the wind functions reported in the literature, two performed reasonably while five others exhibited substantial bias.

Keywords: stream temperature; evaporation; mass transfer model; wind function; latent heat flux

## Introduction

Stream temperature influences aquatic ecosystems through its effects on growth rates (Elliott & Hurley, 1997; Jensen, 1990), species distributions (Ebersole et al., 2001; Parkinson et al., 2016; Wichert & Lin, 1996), and nutrient availability (LeBosquet Jr. & Tsivoglou, 1950). Stream thermal regimes can be modified by natural disturbance such as forest fires (Fried et al., 2004; Isaak et al., 2010; Luce et al., 2014), land use such as forest harvesting (Brown & Krygier, 1970; Guenther et al., 2014), water withdrawals and impoundments (Gu et al., 1998; Hockey et al., 1982; Morse, 1972; Olden & Naiman, 2010), and climatic variability and change (Intergovernmental Panel on Climate Change, 2014; Isaak et al., 2016; Luce et al., 2014). Streams and rivers are exhibiting warming trends in many regions, and there is increasing concern that this warming will have deleterious impacts on cold and cool-water species such as salmon (e.g., Isaak et al., 2018). In response to these concerns, there has been a growth of interest in developing predictive tools to support management decisions using both empirical and process-based approaches (e.g., Fabris et al., 2018; Null et al., 2013).

Process-based stream temperature models provide the most rigorous approach for simulating thermal response to environmental change. Process-based stream temperature modelling is a mature but still developing field. Much of the foundational work was conducted in the 1960s and 1970s (Edinger et al., 1974, 1968). Models have been developed using Lagrangian (Devkota & Imberger, 2012; Gu et al., 1998; Hockey et al., 1982; Vugts, 1974), semi-Lagrangian (Yearsley, 2009), and Eulerian frames of reference (Sinokrot & Stefan, 1993; Sridhar et al., 2004). Methods of solution have ranged from simple Euler integration for Lagrangian models (Hockey et al., 1982; Leach & Moore, 2011) to sophisticated numerical solutions of partial differential equations in a Eulerian framework that are capable of handling unsteady flow (Kim & Chapra, 1997; Younus et al., 2000) and multiple-component transient storage processes (Bingham et al., 2012; Buahin et al., 2019; Cardenas et al., 2014; Meier et al., 2003; Neilson et al., 2010; Westhoff et al., 2010). Even with the increasing complexity and sophistication of numerical schemes for modelling stream thermal processes, the accuracy of stream temperature simulations still depends on accurate modelling of stream surface energy exchanges.

Net radiation is often the dominant surface energy exchange, especially in summer during periods of low flow, when concerns about stream warming are often most acute (Khamis et al., 2015; Leach & Moore, 2010, 2019; Maheu et al., 2014; Morin et al., 1994; Webb & Zhang, 1997). Substantial progress has been made in the development of methods for modelling both shortwave and longwave radiation. For example, the effects of riparian vegetation on shading and the sky view factor can be estimated using hemispherical photographs (Moore

et al., 2005), geometric models (Chen et al., 1998; Li et al., 2012; Moore et al., 2014; Sridhar et al., 2004), and canopy characteristics derived from light detection and ranging (LiDAR) or photogrammetry (Dugdale et al., 2019; Loicq et al., 2018; Richardson et al., 2019). McMahon & Moore (2017) developed an empirical model for computing stream surface albedo as a function of solar angles, turbidity, and aeration.

Less attention has focused on the sensible and latent heat fluxes, despite the fact that latent heat transfer associated with evaporation can be an important heat loss mechanism; studies of stream heat budgets have computed daily losses ranging up to 42 % of the net radiation for a range of sheltered streams (Caissie, 2016; Leach & Moore, 2010; Maheu et al., 2014; Webb & Zhang, 1997). Stream evaporation should increase at higher stream temperatures because of the approximately exponential dependence of surface vapour pressure on water temperature. Therefore, the role of latent heat transfer should become more important as streams and rivers continue to warm, especially in arid regions where streams are not sheltered by riparian forest (Mohseni & Stefan, 1999).

In models for snow and glacier melt, the sensible and latent heat fluxes are commonly computed using semi-empirical bulk aerodynamic formulae, which use air temperature, humidity, and wind speed measurements at one height above the surface, and which explicitly account for measurement height, surface roughness, and atmospheric stability (Conway et al., 2018; Moore, 1983). However, the fetch required to satisfy the underlying assumptions of bulk aerodynamic formulae can be two or more orders of magnitude greater than the measurement height (Oke, 1987). Consequently, these equations are not applicable to small and medium-size streams. As an alternative, stream evaporation is often predicted using empirical mass transfer equations, typically based on the following Dalton-style wind function:

$$E = (a + b \cdot u) \cdot (e_w - e_a) \quad (1)$$

where  $E$  is evaporation rate,  $u$  is wind speed,  $e_w$  and  $e_a$  are the vapour pressures of the water surface and ambient air, respectively, and  $a$  and  $b$  are empirically determined coefficients.

Many stream temperature modelling studies have used wind function models based on energy-balance estimates of evaporation from lakes and ponds (e.g., Brady et al., 1969; King & Neilson, 2019). However, lake- and pond-derived mass transfer models may perform less well when used to estimate stream evaporation due to the lower fetch, especially for sheltered streams (Gulliver & Stefan, 1986; Jobson, 1980). The model with coefficients reported by Webb and Zhang (1997) has been applied with reasonable success to predict stream temperature in a range of studies (e.g., Garner et al., 2014; Leach & Moore, 2011; Magnusson et al., 2012). The Webb-Zhang model appears to have been adapted from the wind function developed by Penman (1956) by applying unit conversions; thus, the Webb-Zhang model

has empirical support based on measurements over a range of “wet” surfaces. Although the coefficients appear to have originated with Penman (1956), they will be called here the “Webb-Zhang” coefficients to avoid confusion with the Penman combination equation for wet-surface evaporation, and in recognition that Webb & Zhang (1997) is the commonly referenced source for those model coefficients.

Empirical mass transfer functions for streams have been derived by energy-balance analysis in three studies focused on artificial or experimental channels (Fulford & Sturm, 1984; Gulliver & Stefan, 1986; Jobson, 1980) and by measuring evaporation using in-stream pans in four studies of natural streams (Benner, 2000; Caissie, 2016; Guenther et al., 2012; Maheu et al., 2014). Guenther et al. (2012), Maheu et al. (2014), and Caissie (2016) each focused on either one or two streams, all in forested catchments, while Benner (2000) focused on nine sites along an arid-land stream in Oregon.

One challenge to comparing stream-derived wind functions is that Jobson (1980), Fulford & Sturm (1984) and Gulliver & Stefan (1986) used meteorological measurements over a land surface, whereas the other studies (i.e., Benner, 2000; Caissie, 2016; Guenther et al., 2012; Maheu et al., 2014) used meteorological measurements over the stream surface. In addition, meteorological measurements were made at different heights. Most studies used measurements made 2 m above the surface, or, as in the case of Gulliver & Stefan (1986), wind speed was measured at 9 m but adjusted to represent measurements at 2 m. Benner (2000) used meteorological data measured 0.5 m above the surface and Guenther et al. (2012) used measurements at 1.5 m above the surface. Even just considering the most comparable studies (Caissie, 2016; Guenther et al., 2012; Maheu et al., 2014), the fitted wind functions varied substantially. For example, the coefficient for wind speed ranged from 0.035 to 0.19  $\text{mm h}^{-1} \text{s m}^{-1} \text{kPa}^{-1}$ . Although some of the variation in fitted wind functions may reflect methodological differences among studies, it could also reflect the effects of site-specific conditions on boundary-layer development over the stream surface, such as atmospheric stability, fetch, and the effects of sheltering by riparian vegetation.

The preceding review indicates that the lack of a robust, spatially transferable model for sensible and latent heat fluxes introduces an as-yet-unquantified source of uncertainty into stream temperature predictions. The broad goal of this study was to contribute to the development of a robust, transferable model of stream evaporation for inclusion in process-based stream temperature models. As a starting point, this research focused on nine forested sites in a temperate mountain region. Evaporation was measured using instream pans over multiple dates and wind functions were fit using above-stream meteorological data at two heights to quantify the effect of measurement height. The candidate models included indices of atmospheric stability and sheltering by forest canopy in order to account explicitly for

these site-specific controls on wind function parameters.

## Methods

### Study sites

Field work was conducted at nine streams in southwest British Columbia, Canada (Figure 1). The streams were distributed between a coastal region and a region approximately 100 km inland (Figure 2). The coastal region has a typical maritime climate with cool, wet winters and mild summers. Mean daily air temperatures at a climate station near the study streams range from 14.9 to 17.7 °C from June to August, with mean total precipitation of 233 mm over the same months. The inland region has relatively colder and drier winters, with warmer and drier summers; mean daily air temperatures from June to August range from 16.3 to 19.2 °C, with a corresponding mean total precipitation of 112 mm. See Table S.1 for more detailed climatic information.

The study sites were selected to sample a range of stream widths, thermal regimes, and riparian vegetation conditions (see Table S.2 in supporting information). The sites were primarily located in coniferous forests, but three stream sites had deciduous trees dominant in their riparian vegetation.

Bankfull width was measured and averaged across three transects at each study site using a 30 m Sokkia/Eslon surveying tape, except at Rutherford Creek where an LTI Impulse 2000 laser rangefinder was used. The transects were spaced such that they bounded the reach where the evaporation pans were deployed. The reach lengths ranged from 5 to approximately 20 m, with longer reaches corresponding to wider streams. Five to six mature trees representative of the local species distribution were selected for tree height measurements; the average was used to characterize each site. Tree height,  $h_t$  (m), was calculated as follows:

$$h_t = HD \times (\tan \theta_p - \tan \theta_n) \quad (2)$$

where HD is the horizontal distance from the measurement location to the tree (m), and  $\theta_t$  and  $\theta_b$  are the angles of inclination, in degrees, from the measurement location to the top and the bottom of the tree, respectively. The horizontal distance was measured using the surveying tape and the angles of inclination were measured using a Suunto PM-5 inclinometer. Canopy openness, as a proportion, was estimated from a hemispherical photograph taken at each site using the image processing software, Gap Light Analyzer (GLA) following the methods detailed by Frazer et al. (1999). The photographs were taken using a Nikon Coolpix 4500 digital camera with a Fisheye Converter FC-E8 lens attached. The camera was mounted

on a tripod and placed in the centre of the stream reach where evaporation and meteorological measurements were made, and levelled prior to taking a photograph. The photographs were taken on days when the sky was uniformly overcast, or in the early morning on days with clear skies.

Stream bankfull widths ranged from 3.1 m to 27.6 m, average tree heights ranged from 5.3 m to 46.7 m, and canopy openness ranged from 9 % to 70 %. Study site elevations ranged from 52 to 1139 masl. The three streams in the interior region drain glacierized catchments and have higher snowmelt contributions, while the coastal region streams have hybrid rain- and snow-dominated hydrologic regimes.

### Stream evaporation measurements

Stream evaporation was measured using the gravimetric approach developed by Maheu et al. (2014). Each evaporation pan consisted of a plastic container with dimensions of  $21.3 \times 21.3 \times 5.1$  cm that was supported by a square wooden frame 34 cm wide, 1.9 cm thick, with an inner opening of  $21.4 \times 21.4$  cm. The frame was painted white to minimize absorption of solar radiation and warming, and was tethered to a concrete anchor to keep it in place when deployed in a stream.

Evaporation measurements were made on 20 days between June 6th and August 17th, 2018; field work was restricted to days without precipitation. On each sampling day, nine evaporation pans were deployed within the channel in pools or locations with low flow velocity. Three pans were placed along each of the left and right banks, and three in the centre of the channel or pool (Figure 3). A preference was given to locations where the evaporation pans could be distributed across the width of the channel, or if that was not feasible, then across the width of a pool.

Each evaporation pan was initially filled with stream water to within about 2 cm of its rim, and then weighed using an Ohaus Scout SPX2201 portable balance (resolution  $\pm 0.1$  g). The mass was measured approximately every 1 to 1.5 hours. The evaporation rate over each measurement interval was computed as

$$E = -\frac{\Delta M \cdot c_f}{\rho_w \cdot A \cdot \Delta t} \quad (3)$$

where  $E$  is evaporation rate ( $\text{mm h}^{-1}$ ) (positive for evaporation, negative for condensation),  $\Delta M$  is the change in mass over the measurement interval (kg),  $\rho_w$  is the density of water ( $\text{kg m}^{-3}$ ),  $\Delta t$  is length of the measurement interval (s),  $A$  is the surface area of the water in the pan ( $\text{m}^2$ ), and  $c_f$  is a conversion factor equal to  $3.6 \cdot 10^6$ , to convert  $E$  from  $\text{m s}^{-1}$  to  $\text{mm h}^{-1}$ . The average evaporation rate over each measurement interval was computed from the nine

pans' evaporation measurements.

Stream temperature was recorded every 10 minutes with an Onset TidbiT v2 water temperature logger, which was housed in a white PVC radiation shield to reduce direct solar radiation effects. The water temperature in each evaporation pan was measured approximately every 20 minutes using an Omega Engineering HH-25TC thermocouple thermometer (resolution  $\pm 0.1$  °C). Temperature measurements were made in the top 1 cm to represent, as closely as possible, temperature at the water surface. A cross-calibration between the TidbiT and the thermocouple was conducted, along with three other water temperature sensors. For the range of temperatures measured in the field, the thermocouple and TidbiT sensor agreed within  $\pm 0.1$  °C for 17 of 24 calibration measurements, and the maximum difference was 0.22 °C. Considering all five sensors, the range of contemporaneous measurements was less than or equal to 0.3 °C for 23 of 24 calibration measurements, with a maximum difference of 0.47 °C.

A continuous record of pan water temperature was generated through linear interpolation from the manual measurements, using the *approx()* function in R (R Core Team, 2019). On days early in the study, when pan water temperature measurements were not made consistently at all pans, the average water temperature difference between the evaporation pans and the stream was used to adjust the recorded stream temperature.

The evaporation pans had slightly curved sides. An empirical model was developed to estimate the surface area of water as a function of mass by setting up a pan on the same scale used to make field measurements. The pan was filled with blue-dyed water in increments of approximately 0.025 kg. After each increment was added, a photograph was taken vertically downward from a camera on a tripod. Surface area was determined for each photograph using the ImageJ software package (Schneider et al., 2012).

### **Above-stream meteorological data collection**

Meteorological conditions 1.5 m and 0.5 m above the stream surface were monitored during evaporation measurements using a Campbell Scientific CR10X data logger. Campbell Scientific HMP45C sensors measured air temperature and relative humidity (RH), with stated accuracies of  $\pm 0.2$  °C and  $\pm 2$  to 3 % RH, respectively, at 20 °C. Wind speed was measured with MetOne 014A 3-cup anemometers, which have nominal starting threshold speeds of 0.45 m s<sup>-1</sup>. Anemometers used in the field were calibrated against two that had been recently serviced by the manufacturer. See Szeitz (2019) for further details.

All sensors were mounted on tripod cross-arms that extended the sensors over the centre of the stream (Figure 3), or in cases where the evaporation pans did not span the full stream width, the sensors were positioned over the centre of the evaporation pans' distribution. The

meteorological sensors were scanned every 10 seconds, and 10-minute averages were logged on a Campbell Scientific CR10X datalogger.

The datalogger was programmed to compute wind speed as  $0.80 \cdot x + 0.447$ , where  $x$  is the pulse-count rate and 0.447 represents the anemometer's stall speed in  $\text{m s}^{-1}$ . An option was enabled such that, if the wind speed was equal to the threshold value (0.447) over a scan period, a value of 0 was returned. Therefore, over 10-minute intervals in which the wind speed was consistently below the threshold value, a value of 0 wind speed was returned. Alternatively, for 10-minute intervals in which there were periods with wind speed both above and below the stall speed, the program could return a wind speed between 0 and  $0.447 \text{ m s}^{-1}$ .

### Calculation of meteorological variables

The saturation vapour pressure,  $e_s(T)$  (kPa), at a temperature  $T$  ( $^{\circ}\text{C}$ ) was computed as:

$$e_s(T) = 0.611 \times \exp\left(\frac{17.27 \cdot T}{T + 237.26}\right) \quad (4)$$

The vapour pressure at the water surface,  $e_w$ , was then computed as:

$$e_w = e_s(T_w) \quad (5)$$

where  $T_w$  is the water temperature of the pan or the stream. The vapour pressure of the air,  $e_a$ , was calculated as:

$$e_a = e_s(T_a) \cdot \frac{RH}{100} \quad (6)$$

where  $T_a$  is the air temperature and  $RH$  is the relative humidity (%). The vapour pressure difference,  $\Delta e$ , driving evaporation was then calculated as:

$$\Delta e = e_w - e_a \quad (7)$$

Two atmospheric stability indices were calculated. For both indices, a value of zero indicates neutral conditions and negative values indicate unstable conditions. One is the virtual temperature difference between the stream surface and the air above it,  $\Delta\theta$  ( $^{\circ}\text{C}$ ), which represents the vertical variation in air density above the stream (Gulliver & Stefan, 1986). The virtual temperature,  $\theta$  (K), of a fluid parcel is calculated as:

$$\theta = \frac{T + 273.15}{1 + 0.378 \cdot e/p} \quad (8)$$

where  $p$  is the atmospheric pressure (kPa),  $e$  is the vapour pressure (kPa) and  $T$  is the

temperature ( $^{\circ}\text{C}$ ) of the fluid, namely the stream or the overlying air. As  $p$  was not measured, a standard pressure,  $P$ , for each field site's elevation was estimated using the U.S. Standard Atmosphere, 1976, atmosphere model (USS, 1976) as follows:

$$P = P_b \cdot \left( \frac{T_b}{T_b + L_b \cdot (h - h_b)} \right)^{\frac{g \cdot M_a}{R^* \cdot L_b}} \times k_p \quad (9)$$

where  $h$  is the elevation of the field site (m), and  $P_b$ ,  $T_b$ ,  $L_b$ , and  $h_b$  are the standard pressure (101.325 kPa), temperature (288.15 K), temperature lapse rate ( $0.0065 \text{ K km}^{-1}$ ), and reference elevation (0 m) where  $0 < h \leq 11,000 \text{ m}$ ;  $g$  ( $\text{m s}^{-2}$ ) is gravitational acceleration,  $M_a$  ( $\text{kg mol}^{-1}$ ) is the molar mass of air,  $R^*$  ( $\text{J mol}^{-1} \text{ K}^{-1}$ ) is the universal gas constant, and  $k_p$  is a conversion factor equal to  $1 \times 10^{-3}$  to convert from units of Pa to kPa. The virtual temperature difference was then calculated as:

$$\Delta\theta = \theta_w - \theta_a \quad (10)$$

where  $\theta_w$  is the virtual temperature at the water surface, and  $\theta_a$  is the virtual temperature of the air above the water.

The second stability index used was the buoyant force,  $\gamma$  ( $\text{m s}^{-2}$ ), which relates buoyant differences to temperature differences between two fluid parcels. It was calculated as:

$$\gamma = g \left( \frac{T_w + 273.15}{T_a + 273.15} - 1 \right) \quad (11)$$

Both stability indices were evaluated as predictors. They performed similarly as predictors, with the buoyant force providing slightly superior performance, so subsequent reference to a stability index will refer solely to the buoyant force.

## Evaluation of models from the literature

We used the data collected in this study to evaluate the performance of wind function models derived in four previous stream-based studies (Benner, 2000; Caissie, 2016; Guenther et al., 2012; Maheu et al., 2014) and two non-stream-based wind functions commonly used in stream temperature models (Brady et al., 1969; Webb & Zhang, 1997). When applying the wind functions of Maheu et al. (2014), Caissie (2016), Brady et al. (1969), and Webb & Zhang (1997) using meteorological data from this study, wind speed data for 1.5 m above the stream were adjusted to 2 m (7 m for the Brady et al. (1969) wind function) using a power-law relation (Sutton, 1953). No adjustments were made to the vapour pressures. For the Benner (2000) model, meteorological measurements made at 0.5 m above the stream were used as

input to be consistent with the measurements in that study.

For comparison to the literature models, we fit a “base” model of the form of Eq. 1 to our data. Whereas previous studies fit wind function models separately by site, models were fit in this study to the full data set using mixed-effects statistical models. Mixed-effects models are based on the assumption that there is a set of fixed-effects coefficients that apply throughout the population of sites to which the model is intended to apply, and that the coefficients at any given site exhibit random deviations from the fixed-effects values. As applied in this study, the goal of mixed-effects models is to derive the best model that could be applied to new sites with no additional calibration. Mixed-effects models are common in biological science and ecology, but have had fewer applications in hydrology; some hydrological examples include Booker & Dunbar (2008), Kasurak et al. (2011), Ploum et al. (in press) and Howie et al. (2020).

When framed as a mixed-effects model, the base wind function model can be expressed as

$$E_{ik} = (a + \alpha_k) \cdot (e_{w,ik} - e_{a,ik}) + (b + \beta_k) \cdot w_{ik} \cdot (e_{w,ik} - e_{a,ik}) + \epsilon_{ik} \quad (12)$$

where the subscript  $k$  indicates a specific site; the subscript  $i$  indicates the  $i^{th}$  observation at site  $k$ ;  $a$  and  $b$  are fixed effects that are assumed to apply to the entire population of sites;  $\alpha_k$  and  $\beta_k$  are deviations from the fixed-effects coefficients for site  $k$ , assumed to be drawn from normally distributed populations; and  $\epsilon_{ik}$  is a random error term. If the model were applied to a new site, only the fixed-effects coefficients ( $a$  and  $b$ ) would be used. If the model were applied to new observations from one of the original sites, then both the fixed effects and the random effects for that site ( $\alpha_k$  and  $\beta_k$ ) would be used.

The performance of the fitted models was evaluated using leave-one-site-out cross-validation. In each iteration of the cross-validation, all data for one site were withheld; the model was fit using data for the remaining sites and then applied using the fixed-effects coefficients to data for the withheld site. Model performance was determined by computing the root-mean-square error ( $RMSE$ ,  $\text{mm h}^{-1}$ ) and the Nash-Sutcliffe efficiency ( $NSE$ ), as follows:

$$RMSE = \sqrt{\frac{1}{n} \sum_{i=1}^n (\hat{E}_i - E_i)^2} \quad (13)$$

$$NSE = 1 - \frac{\sum_{i=1}^n (\hat{E}_i - E_i)^2}{\sum_{i=1}^n (E_i - \bar{E})^2} \quad (14)$$

where  $\hat{E}_i$  is the modelled evaporation rate, and  $\bar{E}$  is the mean observed evaporation rate from the nine pans for a given measurement interval.

To evaluate the sensitivity of the results to uncertainties in the pan temperatures, the model comparison was conducted using both the recorded ambient stream temperature and the interpolated pan water temperature to determine  $e_w$ .

## Evaluation of extended models and effect of measurement height

In addition to applying the base model, we tested the performance of extended models that included additional predictors. Specifically, canopy openness ( $\phi$ ) and buoyant force ( $\gamma$ ) were incorporated as additional model predictors in various combinations to form a total of 12 candidate models as listed in Table 1.

Separate models were fit for each of the two measurement heights (0.5 m and 1.5 m). The 12 expanded models listed in Table 1 were fit using the mixed-effects approach described above, and with surface vapour pressure computed using the interpolated pan water temperatures. In the first round of model testing, the mixed-effects models allowed each model parameter, ( $a$ ,  $b$ , and if present,  $c$  and  $d$ ), to vary by site. Any model that had one or more insignificant estimated fixed-effects coefficients (p-value > 0.05) was dropped from further consideration.

## Results

### Evaporation pan water temperature

For eight of the nine streams, water in the evaporation pans averaged between 0.51 and 1.64 °C warmer than stream temperature. The exception was Marion Creek, however, which had consistently lower pan water temperatures with an average difference of -0.66 °C (Figure 4). The trend in the water temperature difference typically followed the stream temperature trend, but there was variability among pans depending on their exposure to solar radiation (Figure S.1). Individual openings in the canopy provided localized pools of sunlight to the stream, which increased the water temperature of any evaporation pans they crossed over the course of a day. The full daily time series of stream and evaporation pan temperatures can be found in the Supporting Information (Figure S.2).

### Meteorological conditions and evaporation rates

The distributions of measured and derived meteorological conditions, and the measured evaporation rates, are presented in Figure 5. The meteorological and stream temperature data are at 10-minute intervals, and the evaporation rate measurements are at approximately 1- to 1.5-hour intervals. Time series of meteorological data are provided in the Supporting

Information (Figure S.3).

As seen in Figure 5 (top panel) and in the supporting information (Figure S.3), air temperatures were typically greater than stream temperature, and increased with height above the stream surface (Figure 6, top panel). Exceptions to this trend were observed at Marion Creek and Blaney Creek (Lower), as the former had higher stream temperatures than air temperatures at almost all times, and the latter experienced several hours of nearly equal stream and air temperatures on July 5th. Both of these study sites are downstream of lakes that are subject to substantial warming.

Measured wind speeds often increased with height above the stream surface but not consistently (see Figure 6, middle panel, and supporting information, Figure S.3). A generally negative relation exists between the average difference in wind speeds, the local canopy openness, and the sheltering ratio. As seen in Table 2, both of the Blaney Creek sites and Spring Creek have sheltering ratio values  $> 4$  and canopy openness values  $< 0.25$ , and they experienced the greatest average wind speed differences, ranging from  $0.12$  to  $0.22 \text{ m s}^{-1}$ . Conversely, Alouette River and Miller Creek have low sheltering ratios ( $< 1$ ) and greater canopy openness values ( $> 0.50$ ), and they experienced average wind speed differences of approximately  $0.02 \text{ m s}^{-1}$ .

The vapour pressure at  $0.5 \text{ m}$  was greater than the vapour pressure at  $1.5 \text{ m}$  for 95 % of the observations (Figure 6, bottom panel); see also Supporting Information (Figure S.3). The greatest vapour pressure differences were associated with the highest stream temperatures, as observed at Marion Creek and Alouette River (Figure 5).

Conditions were generally stable, with unstable conditions indicated for only 12 to 14 % of the time at heights of  $1.5$  and  $0.5 \text{ m}$ , respectively. The exception to this trend was Marion Creek; it was dominated by unstable conditions, which occurred  $> 97$  % of the time, at both heights.

Evaporation rates ranged from  $-0.01$  to  $0.20 \text{ mm h}^{-1}$  with a mean evaporation rate of  $0.06 \text{ mm h}^{-1}$  (Figure 5). As expected, evaporation rates generally increased with increasing vapour pressure differences and/or higher wind speed (e.g. comparing Alouette River to Marion Creek, Figure 5 panel 4).

An error analysis indicated that the mean uncertainty in the measured evaporation rate for an individual pan measurement was  $0.004 \text{ mm h}^{-1}$  (see Supporting Information). The uncertainty in the mean evaporation rate, as represented by a statistical confidence interval around the mean, was greater than the measurement uncertainty for an individual pan. Indeed, for three observations of low evaporation rates, the 95 % confidence intervals were greater than the magnitude of the observations (Figure S.4). This result indicates that sampling variability was often substantially greater than the uncertainty of an individual pan

measurement. The median relative uncertainty in mean evaporation was 13 %.

## Literature wind function comparison

Fitted model coefficients vary substantially among studies (Table 3). Relative model performance was consistent regardless of whether the  $e_w$ , and by extension the  $\Delta e$ , was computed using the stream or the pan water temperature (Figure 7). However, performance of the fitted models, and those of Brady et al. (1969) and Webb & Zhang (1997), was slightly better when using the interpolated pan temperatures.

As seen in Figure 7, the models of Benner (2000) and Maheu et al. (2014) consistently overestimated evaporation, the model of Caissie (2016) overestimated on average but had high variability, and the model of Guenther et al. (2012) consistently underestimated evaporation. Both the Brady et al. (1969) and Webb and Zhang (1997) models performed similarly to this study's base model (Figure 8).

## Effects of additional predictors and measurement height

Of the model forms in Table 1, no model that expanded upon the base mass transfer model with a stability index alone was significant. Models that expanded upon the base model with a canopy openness variable alone were only significant when the canopy variable was an interaction term on the wind speed. Models that included both a stability and canopy variable often had multiple forms that were fully significant.

The results of the cross-validation of the significant models are summarized in Table 4. Model performance was considered on the basis of the root-mean-square error, and the best performing models' estimated coefficients are provided in Table 5. The base model performed well under cross-validation for both the 0.5-m and 1.5-m measurements; the 0.5-m model had a root-mean-square error (RMSE) of 0.0162 mm h<sup>-1</sup> and a Nash-Sutcliffe efficiency of 0.897, while the 1.5-m model had respective values of 0.0187 mm h<sup>-1</sup> and 0.862.

Of the models based on 1.5-m measurements that had significant coefficients, 72 % improved upon the performance of the base model under cross-validation compared to 29 % for the filtered 0.5-m models. The best performing expanded model fit to the 0.5-m measurements, Model 9, provided a 2 % reduction in the RMSE from the base model. The best performing expanded model fit to the 1.5-m measurements, Model 11, provided an 11 % reduction in the RMSE. The cross-validated model predictions for the selected models in Table 1 are shown in Figure 8. While the expanded 0.5-m model had better goodness-of-fit indicators than the expanded 1.5-m model, they both had similar site-specific residual error distributions, with the exception of the streams draining glacierized catchments (Cayoosh Creek, Miller Creek,

Rutherford Creek) as seen in Figure 9.

While the fixed-effects coefficients are used during model cross-validation and when applying the models to external datasets, the magnitudes of the site-specific adjustments for a given model provide information on how much site-specific variability is not accounted for by the fixed-effects terms in the model. The base model's site-specific adjustments ranged from 0.4 to 37 % of the fixed-effect coefficient value for the 1.5-m model, and between 1 and 25 % for the 0.5-m model. This result indicates that there was site-specific variability unaccounted for by the base model predictors, especially for the 1.5-m model. However, the expanded models' site-specific adjustments were less than 0.001 % of the fixed-effect coefficient value for both the 1.5-m and 0.5-m models. That is, explicitly incorporating canopy openness and stability predictors into the model effectively accounted for the site-specific variability that was otherwise accounted for through site-specific random-effects adjustments to the wind function.

## Discussion

### Assessment of evaporation pan methodology

Overall uncertainty in the mean evaporation rate for a given measurement interval, as expressed in the confidence limits around the mean, is a combination of random measurement error and sampling variability. Given the design of the pans and their mode of deployment in this study, each pan was able to provide an estimate of evaporation with a mean uncertainty of  $0.004 \text{ mm h}^{-1}$ , relative to mean and maximum measured rates of  $0.06$  and  $0.20 \text{ mm h}^{-1}$ , respectively. However, the confidence limits for the mean evaporation were generally greater than the uncertainty in an individual pan measurement, suggesting that sampling variability was the dominant source of uncertainty. Sampling variability arises because the pans experienced variable conditions caused, for example, by differences in pan water heating due to sunlight infiltrating canopy gaps, or differences in wind exposure due to in-stream boulders or overhanging vegetation. While the overall uncertainty increased with increasing mean evaporation rates, its relative magnitude decreased. For example, the mean overall uncertainty was 27 % of the mean evaporation rate at Miller Creek ( $0.006 \text{ mm h}^{-1}$  and  $0.022 \text{ mm h}^{-1}$ , respectively), while the mean overall uncertainty at Rutherford Creek was 7.6 % of the mean evaporation rate ( $0.010 \text{ mm h}^{-1}$  and  $0.136 \text{ mm h}^{-1}$ , respectively). Considering all streams, the results indicate that an overall uncertainty of approximately 18 % of the mean measured value can be achieved for typical conditions by deploying nine evaporation pans. This result highlights the need for replication of pans to achieve an appropriate level of

accuracy.

The water temperature in the evaporation pans often differed substantially from that of the stream, ranging from 1.4 °C lower to 4.5 °C higher than stream temperature. The time series of pan water temperatures show that frequent temperature fluctuations occurred within measurement intervals, and warming occurred within 10 to 20 minutes of pan deployment on numerous occasions (Supporting Information, Figure S.2). If this temperature difference were not accounted for, the vapour pressure difference used in the wind function would often be underestimated, potentially leading to an overestimate of the fitted wind function coefficients, as seen in Table 3.

Given the observed rates of pan warming, it is recommended that future users of this methodology measure the surface temperature of the water in the evaporation pans with high temporal resolution (e.g., every 10 minutes). In addition, it may be useful to experiment with alternative materials. The pans used in this study were made from plastic with a recycling code of 5, indicating polypropylene. Published thermal conductivities for polypropylene range from 0.10 to 0.22 W m<sup>-1</sup> °C<sup>-1</sup> (Engineering Toolbox, 2003). For comparison, aluminum has a thermal conductivity of approximately 240 W m<sup>-1</sup> °C<sup>-1</sup> (Engineering Toolbox, 2003).

It was only possible to deploy the pans at sites with placid flow, and the water in the pans was not moving. Based on a limited set of experiments, Benner (2000) found that evaporation from moving water was greater than that for still water at low wind speeds with low vapour pressure differences. However, these conditions are associated with low evaporation; Benner (2000) found minimal difference in evaporation from still and moving water for conditions conducive to higher evaporation. A more serious limitation relates to the potential effect of aeration on evaporation. Aerated water has a greater effective surface area than water with placid flow, which could enhance sensible and latent heat exchanges. Therefore, there is some question about the applicability of the fitted wind functions to steep streams, especially at higher flows when aeration becomes stronger.

## Meteorological data measurement height and instrument sensitivity

Previous studies used measurement heights of 1.5 or 2 m, with the exception of Benner (2000), who used a measurement height of 0.5 m. In this study, the  $a$  coefficient for the 0.5 m measurement height (0.0815 mm h<sup>-1</sup> kPa<sup>-1</sup>) was higher than that for the 1.5 m measurement height (0.0663 mm h<sup>-1</sup> kPa<sup>-1</sup>), while the  $b$  coefficient was similar between the two measurement heights. The increased value of  $a$  with decreased measurement height is consistent with the fact that the vapour pressure difference driving evaporation should decrease

with decreasing measurement height, as was the case for the majority of measurements.

Model performance was better when using meteorological measurements from 0.5 m rather than 1.5 m above the stream surface, producing a 13 % reduction in root-mean-square error for the base model. This superior performance could result from the fact that measurements at a lower height would be closer to being in an internal boundary layer adjusted to the water surface. Although this result might encourage the use of lower measurement heights, an important consideration is that stream stage varies with discharge; this point is particularly relevant for proglacial streams, which experience significant diel fluctuations in discharge. As a consequence, wind functions derived from measurements at a specific height would not be accurate when applied to streams with varying stages with meteorological measurements at a fixed height. As the gradients of wind speed and vapour pressure tend to decrease with increasing height above a surface, this source of error would be greatest for wind functions derived from measurements at a low height. A further consideration relates to instrument precision. Because wind speed and surface-to-air vapour pressure differences generally increase with height above a stream, these measured values should be subject to less relative uncertainty when measured at a greater height above the stream surface.

Given the starting-speed limitations of the cup-type anemometers often employed for meteorological measurements, low wind speeds are likely to be under-reported for sheltered streams. In cases where the wind-function intercept is non-zero, the model implicitly adjusts for the effect of the anemometer's stall speed on the estimated coefficient values. However, if these models were applied using wind speed data obtained from a sensor with increased accuracy (lower starting/stalling speed), the predictions would be biased for low wind speeds. Empirically derived wind functions must be applied with consideration of the accuracy of the instruments used to obtain the fitting data in order to produce reliable and unbiased estimates.

### **Effects of additional predictor variables**

For both meteorological measurement heights, the addition of a stability variable alone was either not significant or did not improve model predictions. For measurements made at 1.5 m, the addition of canopy and stability variables together provided modest model improvement, with an 11 % reduction in root-mean-square error and an increase in the Nash-Sutcliffe efficiency from 0.862 to 0.891. However, for measurements made at 0.5 m, the addition of a canopy variable alone outperformed the addition of both variables, but provided marginal improvements over the base model (2 % reduction in root-mean-square error, increased Nash-Sutcliffe efficiency from 0.897 to 0.900).

The relatively minor improvement associated with the expanded models suggests that stability played a minor role compared to the forced convection influence of wind on vapour transfer for these small, relatively sheltered streams. However, the limited range of stability conditions observed in the current study may have been insufficient to comprehensively evaluate its influence. The benefit of adding stability and/or canopy openness predictors for both measurement heights is that they account for the site-to-site variability that could not be accounted for by the base model. While the stability index can be computed from air and stream temperatures, canopy openness is not typically available. Where field measurements are not available, canopy openness could be estimated using satellite imagery (Carreiras et al., 2006), LiDAR data (Korhonen et al., 2011) or photogrammetry (Dugdale et al., 2019). Given these concerns and those discussed in the previous section, it is recommended that the expanded 1.5 m model be used if canopy openness measurements are available, or reliable estimates can be obtained, given its superior performance over the base model.

### **Comparison of wind function coefficients among studies and scope of application**

Most studies of stream evaporation focused on one or at most two streams and produced site-specific estimates of the wind function coefficients (Table 3). Interestingly, the models developed using stream evaporation measurements performed relatively poorly when applied to our data, with both consistent overestimation (Benner, 2000) and underestimation (Guenther et al., 2012). On the other hand, both the Brady et al. (1969) and Webb & Zhang (1997) models came close to matching the performance of this study's base model, despite not being based on stream evaporation measurements.

Based on the cross-validation results, the models developed in this study can provide estimates of evaporation with a typical error of less than  $0.02 \text{ mm h}^{-1}$  or, in energy flux units, about  $14 \text{ W m}^{-2}$ . The cross-validation results indicate that the models can be applied with reasonable confidence to model water temperature for small- to medium-size streams in temperate forested landscapes. However, the model developed by Benner (2000) overestimated evaporation for our field sites, which suggests that the models developed in this study would underestimate evaporation at the field sites studied by Benner (2000), which were located in a warmer, drier environment. It is recommended that future research on stream evaporation apply a consistent methodology to streams representing a broad range of thermal regimes, physiography, and hydroclimate.

A challenge in applying wind functions for computing the sensible and latent heat fluxes for streams is generating suitable meteorological data. Above-stream conditions differ from

those over land, typically being cooler and moister during daytime in summer and less windy for sheltered sites (Benyahya et al., 2010; Guenther et al., 2012; Leach & Moore, 2010). Consequently, if wind functions derived using above-stream meteorological data were applied using land-based meteorological measurements, the simulated sensible and latent heat fluxes would be biased. On the other hand, if wind functions are fit using land-based meteorological data (e.g., Fulford & Sturm, 1984; Gulliver & Stefan, 1986; Jobson, 1980), then the fitted coefficients implicitly incorporate the effects of sheltering and internal boundary layer development over the surface of the study stream, which could limit the applicability of the wind function to other sites.

In most applications of stream temperature models, meteorological data are measured at land-based stations. There have been attempts to develop empirical approaches for using land-based meteorological data to predict evaporation as a function of fetch or surface area (Granger & Hedstrom, 2011; McJannet et al., 2012). While these approaches may be reasonable for lakes and ponds, they may be less applicable for streams, given their distinctive linear geometry and the influences of stream banks and riparian vegetation on boundary-layer development.

Future research should focus on developing approaches to adjust such land-based measurements to make them consistent with above-stream conditions to reduce bias. As a starting point, it may be useful to scale temperature and vapour pressure as  $(x_a - x_w)/(x_l - x_w)$ , where  $x$  represents one of air temperature or vapour pressure, and the subscripts  $a$ ,  $w$ , and  $l$  indicate conditions above the stream, at the water surface and at a land-based weather station, respectively. For wind speed, an appropriate scaling could be  $u_a/u_l$ . These scaled variables could then be related to variables such as stream width and vegetation height. Considering the current paucity of above-stream meteorological data, there is a need for further field work to collect relevant data over a range of streams to support the development of empirical scaling relations. This field work should be supported by theoretical work that expands upon earlier lake- and pond-focused studies by Weisman & Brutsaert (1973) and Hipsey & Sivapalan (2003), but which explicitly accounts for distinctive features of streams.

## Conclusion

Evaporation rates were measured using floating evaporation pans at nine streams with a range of widths (3.1 to 27.6 m), temperature regimes, and degrees of sheltering. The evaporation rates ranged from  $-0.01$  to  $0.20$  mm h<sup>-1</sup>, with a mean rate of  $0.06$  mm h<sup>-1</sup>. Generalized wind functions were derived using these measurements and meteorological conditions measured 1.5 and 0.5 m above the stream surface, and had respective root-mean-square errors of 0.0187

and  $0.0162 \text{ mm h}^{-1}$  under cross-validation, and respective Nash-Sutcliffe efficiencies of 0.862 and 0.897. The cross-validation results support the application of the fitted models for small- to medium-size streams in temperate forested regions.

Canopy openness and a stability index, the buoyant force, were incorporated as additional model predictors. The addition of a stability predictor alone did not improve model predictions. The wind function had consistent performance under cross-validation, and the addition of canopy openness and stability predictors reduced site-specific variability in evaporation predictions. The reductions in prediction error achieved with these additional variables were greater for measurements at 1.5 m rather than 0.5 m. The wind function models presented by Brady et al. (1969) and Webb & Zhang (1997) performed similarly to models fit specifically to our data set.

Future research should investigate stream evaporation using a consistent methodology across a broader range of conditions (stream temperatures, widths, degrees of sheltering, and stability conditions), as well as examining the nature of wind, temperature, and humidity profiles above streams. This would advance our understanding of stream evaporation in complex micrometeorological environments and the variability in wind function coefficients, and would aid the development of more robust, generalized wind functions applicable to a broader range of streams. In addition, further research should focus on the effect of aeration on sensible and latent heat exchanges.

## Data availability statement

The data that support the findings of this study are openly available in Zenodo at <http://doi.org/10.5281/zenodo.3592942>.

## References

1976. *U.S. Standard Atmosphere, 1976*. National Oceanic and Atmospheric Administration and the National Aeronautics and Space Administration and the United States Air Force, Washington, D.C.
- Benner, DA, 2000. Evaporative heat loss of the Upper Middle Fork of the John Day River, Northeastern Oregon. Master's thesis, Oregon State University.
- Benyahya, L, Caissie, D, El-Jabi, N, & Satish, MG, 2010. Comparison of microclimate vs. remote meteorological data and results applied to a water temperature model (Miramichi River, Canada). *Journal of Hydrology* **380**: 247–259. doi:10.1016/j.jhydrol.2009.10.039.

- Bingham, QG, Neilson, BT, Neale, CMU, & Cardenas, MB, 2012. Application of high-resolution, remotely sensed data for transient storage modeling parameter estimation. *Water Resources Research* **48**. doi:10.1029/2011WR011594.
- Booker, DJ & Dunbar, MJ, 2008. Predicting river width, depth and velocity at ungauged sites in England and Wales using multilevel models. *Hydrological Processes* **22**. doi:10.1002/hyp.7007.
- Brady, DK, Graves, WL, & Geyer, JC, 1969. Surface heat exchange at power plant cooling lakes. In: *Cooling water discharge project report No. 5*. Edison Electric Institute, New York.
- Brown, GW & Krygier, JT, 1970. Effects of clear-cutting on stream temperature. *Water Resources Research* **6**: 1133–1139. doi:10.1029/WR006i004p01133.
- Buahin, CA, Horsburgh, JS, & Neilson, BT, 2019. Parallel multi-objective calibration of a component-based river temperature model. *Environmental Modelling & Software* **116**: 7–71. doi:10.1016/j.envsoft.2019.02.012.
- Caissie, D, 2016. River evaporation, condensation and heat fluxes within a first-order tributary of Catamaran Brook (New Brunswick, Canada). *Hydrological Processes* **30**: 1872–1883. doi:10.1002/hyp.10744.
- Cardenas, MB, Doering, M, Rivas, DS, Galdeano, C, Neilson, BT, & Robinson, CT, 2014. Analysis of the temperature dynamics of a proglacial river using time-lapse thermal imaging and energy balance modeling. *Journal of Hydrology* **519**: 1963–1973. doi:10.1016/j.jhydrol.2014.09.079.
- Carreiras, JMB, Pereira, JMC, & Pereira, JS, 2006. Estimation of tree canopy cover in evergreen oak woodlands using remote sensing. *Forest Ecology and Management* **223**: 45–53. doi:10.1016/j.foreco.2005.10.056.
- Chen, YD, Carsel, RF, McCutcheon, SC, & Nutter, WL, 1998. Stream temperature simulation of forested riparian areas: I. Watershed-scale model development. *Journal of Environmental Engineering* **124**: 304–315. doi:10.1061/(ASCE)0733-9372(1998)124:4(304).
- Conway, JP, Pomeroy, JW, Helgason, WD, & Kinar, NJ, 2018. Challenges in modeling turbulent heat fluxes to snowpacks in forest clearings. *Journal of Hydrometeorology* **19**: 1599–1616. doi:10.1175/JHM-D-18-0050.1.
- Devkota, B & Imberger, J, 2012. Upper and Middle Tiete River Basin dam-hydraulic

- system, travel time and temperature modeling. *Journal of Hydrology* **475**: 12–25. doi:10.1016/j.jhydrol.2012.07.025.
- Dugdale, SJ, Malcolm, IA, & Hannah, DM, 2019. Drone-based Structure-from-Motion provides accurate forest canopy data to assess shading effects in river temperature models. *Science of The Total Environment* **678**: 326–340. doi:10.1016/j.scitotenv.2019.04.229.
- Ebersole, JL, Liss, WJ, & Frissell, CA, 2001. Relationship between stream temperature, thermal refugia and rainbow trout *Oncorhynchus mykiss* abundance in arid-land streams in the northwestern United States. *Ecology of Freshwater Fish* **10**: 1–10. doi:10.1034/j.1600-0633.2001.100101.x.
- Edinger, JE, Brady, DK, & Geyer, JC, 1974. Heat exchange and transport in the environment. Report 14, Electric Power Research Institute, Palo Alto, California.
- Edinger, JE, Brady, DK, & Graves, WL, 1968. The variation of water temperatures due to steam electric cooling operations. *Journal of the Water Pollution Control Federation* **40**: 1632–1639.
- Elliott, JM & Hurley, MA, 1997. A functional model for maximum growth of Atlantic Salmon parr, *Salmo salar*, from two populations in northwest England. *Functional Ecology* **11**: 592–603. doi:10.1046/j.1365-2435.1997.00130.x.
- Engineering Toolbox, 2003. Thermal conductivity of selected materials and gases. Accessed 2020-02-17.
- Fabris, L, Malcolm, I, & Buddendorf, WB, 2018. Integrating process-based flow and temperature models to assess riparian forests and temperature amelioration in salmon streams. *Hydrological Processes* **32**: 776–791. doi:10.1002/hyp.11454.
- Frazer, GW, Canham, CD, & Lertzman, KP, 1999. *Gap Light Analyzer (GLA) Version 2.0: Imaging software to extract canopy structure and gap light transmissions indices from true-colour fisheye photographs, users manual and program documentation*.
- Fried, JS, Torn, MS, & Mills, E, 2004. The impact of climate change on wildfire severity: a regional forecast for Northern California. *Climatic Change* **64**: 169–191.
- Fulford, JM & Sturm, TW, 1984. Evaporation from flowing channels. *Journal of Energy Engineering* **110**: 1–9.
- Garner, G, Malcolm, IA, Sadler, JP, & Hannah, DM, 2014. What causes cooling water temperature gradients in a forested stream reach? *Hydrology and Earth System Sciences* **18**: 5361–5376. doi:10.5194/hess-18-5361-2014.

- Granger, RJ & Hedstrom, N, 2011. Modelling hourly rates of evaporation from small lakes. *Hydrology and Earth System Sciences* **15**: 267–277. doi:10.5194/hess-15-267-2011.
- Gu, R, Montgomery, S, & Austin, TA, 1998. Quantifying the effects of stream discharge on summer river temperature. *Hydrological Sciences Journal* **43**: 885–904.
- Guenther, SM, Gomi, T, & Moore, RD, 2014. Stream and bed temperature variability in a coastal headwater catchment: influences of surface-subsurface interactions and partial-retention forest harvesting. *Hydrological Processes* **28**: 1238–1249. doi:10.1002/hyp.9673.
- Guenther, SM, Moore, RD, & Gomi, T, 2012. Riparian microclimate and evaporation from a coastal headwater stream, and their response to partial-retention forest harvesting. *Agricultural and Forest Meteorology* **164**: 1–9. doi:10.1016/j.agrformet.2012.05.003.
- Gulliver, JS & Stefan, HG, 1986. Wind function for a sheltered stream. *Journal of Environmental Engineering* **112**: 387–399.
- Hipsey, MR & Sivapalan, M, 2003. Parameterizing the effect of a wind shelter on evaporation from small water bodies. *Water Resources Research* **39**. doi:10.1029/2002WR001784.
- Hockey, JB, Owens, IF, & Tapper, NJ, 1982. Empirical and theoretical models to isolate the effect of discharge on summer water temperatures in the Hurunui River. *Journal of Hydrology (New Zealand)* **21**: 1–12.
- Howie, SA, Whitfield, PH, & Moore, RD, 2020. Plant community type is an indicator of the seasonal moisture deficit in a disturbed raised bog. *Ecohydrology* **13**(4). doi:10.1002/eco.2209.
- Intergovernmental Panel on Climate Change, 2014. *Climate change 2013 – the physical science basis: working group I contribution to the fifth assessment report of the Intergovernmental Panel on Climate Change*. Cambridge University Press. doi:10.1017/CBO9781107415324.
- Isaak, DJ, Luce, CH, Horan, DL, Chandler, GL, Wollrab, SP, & Nagel, DE, 2018. Global warming of salmon and trout rivers in the northwestern U.S.: road to ruin or path through purgatory? *Transactions of the American Fisheries Society* **147**: 566–587. doi:10.1002/tafs.10059.
- Isaak, DJ, Luce, CH, Rieman, BE, Nagel, DE, Peterson, EE, Horan, DL et al., 2010. Effects of climate change and wildfire on stream temperatures and salmonid thermal habitat in a mountain river network. *Ecological Applications* **20**: 1350–1371. doi:10.1890/09-0822.1.
- Isaak, DJ, Young, MK, Luce, CH, Hostetler, SW, Wenger, SJ, Peterson, EE et al., 2016. Slow climate velocities of mountain streams portend their role as refugia for cold-water

- biodiversity. *Proceedings of the National Academy of Sciences of the United States of America* **113**: 4374–4379. doi:10.1073/pnas.1522429113.
- Jensen, AJ, 1990. Growth of young migratory brown trout *Salmo trutta* correlated with water temperature in Norwegian rivers. *Journal of Animal Ecology* **59**: 603–614. doi:10.2307/4883.
- Jobson, HE, 1980. Thermal modeling of flow in the San Diego Aqueduct, California, and its relation to evaporation. United states geological survey professional paper 1122, US Department of Interior, Washington, DC.
- Kasurak, A, Kelly, R, & Brenning, A, 2011. Linear mixed modelling of snow distribution in the central Yukon. *Hydrological Processes* **25**: 3332–3346. doi:10.1002/hyp.8168.
- Khamis, K, Brown, LE, Milner, AM, & Hannah, DM, 2015. Heat exchange processes and thermal dynamics of a glacier-fed alpine stream. *Hydrological Processes* **29**: 3306–3317. doi:10.1002/hyp.10433.
- Kim, KS & Chapra, SC, 1997. Temperature model for highly transient shallow streams. *Journal of Hydraulic Engineering* **123**: 30–40. doi:10.1061/(ASCE)0733-9429(1997)123:1(30).
- King, TV & Neilson, BT, 2019. Quantifying reach-average effects of hyporheic exchange on Arctic river temperatures in an area of continuous permafrost. *Water Resources Research* **55**: 1951–1971. doi:10.1029/2018WR023463.
- Korhonen, L, Korpela, I, Heiskanen, J, & Maltamo, M, 2011. Airborne discrete-return LIDAR data in the estimation of vertical canopy cover, angular canopy closure and leaf area index. *Remote Sensing of Environment* **115**: 1065–1080. doi:10.1016/j.rse.2010.12.011.
- Leach, JA & Moore, RD, 2010. Above-stream microclimate and stream surface energy exchanges in a wildfire-disturbed riparian zone. *Hydrological Processes* **24**: 2369–2381. doi:10.1002/hyp.7639.
- Leach, JA & Moore, RD, 2011. Stream temperature dynamics in two hydrogeomorphically distinct reaches. *Hydrological Processes* **25**: 679–690. doi:10.1002/hyp.7854.
- Leach, JA & Moore, RD, 2019. Empirical stream thermal sensitivities may underestimate stream temperature response to climate warming. *Water Resources Research* **55**. doi:10.1029/2018WR024236.
- LeBosquet, M, Jr. & Tsivoglou, EC, 1950. Simplified dissolved oxygen computations. *Sewage and Industrial Wastes* **22**: 1054–1061.

- Li, G, Jackson, CR, & Kraseski, KA, 2012. Modeled riparian stream shading: agreement with field measurements and sensitivity to riparian conditions. *Journal of Hydrology* **428-429**: 142–151. doi:10.1016/j.jhydrol.2012.01.032.
- Loicq, P, Moatar, F, Jullian, Y, Dugdale, SJ, & Hannah, DM, 2018. Improving representation of riparian vegetation shading in a regional stream temperature model using LiDAR data. *Science of The Total Environment* **624**: 480–490. doi:10.1016/j.scitotenv.2017.12.129.
- Luce, C, Staab, B, Kramer, M, Wenger, S, Isaak, D, & McConnell, C, 2014. Sensitivity of summer stream temperatures to climate variability in the Pacific Northwest. *Water Resources Research* **50**: 3428–3443. doi:10.1002/2013WR014329.
- Magnusson, J, Jonas, T, & Kirchner, JW, 2012. Temperature dynamics of a proglacial stream: identifying dominant energy balance components and inferring spatially integrated hydraulic geometry. *Water Resources Research* **48**. doi:10.1029/2011WR011378.
- Maheu, A, Caissie, D, St-Hilaire, A, & El-Jabi, N, 2014. River evaporation and corresponding heat fluxes in forested catchments. *Hydrological Processes* **28**: 5725–5738. doi:10.1002/hyp.10071.
- McJannet, DL, Webster, IT, & Cook, FJ, 2012. An area-dependent wind function for estimating open water evaporation using land-based meteorological data. *Environmental Modelling & Software* **31**: 76–83. doi:10.1016/j.envsoft.2011.11.017.
- McMahon, A & Moore, RD, 2017. Influence of turbidity and aeration on the albedo of mountain streams. *Hydrological Processes* **31**: 4477–4491. doi:10.1002/hyp.11370.
- Meier, MF, Dyurgerov, MB, & McCabe, GJ, 2003. The health of glaciers: recent changes in glacier regime. *Climatic Change* **59**: 123–135.
- Mohseni, O & Stefan, HG, 1999. Stream temperature-air temperature relationships: a physical interpretation. *Journal of Hydrology* **218**: 128–141. doi:10.1016/S0022-1694(99)00034-7.
- Moore, RD, 1983. On the use of bulk aerodynamic formulae over melting snow. *Nordic Hydrology* **14**: 193–206. doi:10.2166/nh.1983.0016.
- Moore, RD, Leach, JA, & Knudson, JM, 2014. Geometric calculation of view factors for stream surface radiation modelling in the presence of riparian forest. *Hydrological Processes* **28**: 2975–2986. doi:10.1002/hyp.9848.
- Moore, RD, Spittlehouse, DL, & Story, A, 2005. Riparian microclimate and stream temperature response to forest harvesting: a review. *Journal of the American Water Resources Association* **41**: 813–834. doi:10.1111/j.1752-1688.2005.tb03772.x.

- Morin, G, Nzakimuena, TJ, & Sochanski, W, 1994. Pr evision des temp eratures de l'eau en rivi eres   l'aide d'un mod ele conceptuel: le cas de la rivi ere Moisie. *Canadian Journal of Civil Engineering* **21**: 63–75.
- Morse, WL, 1972. Stream temperature prediction under reduced flow. *Journal of the Hydraulics Division* **98**: 1031–1047.
- Neilson, BT, Stevens, DK, Chapra, SC, & Bandaragoda, C, 2010. Two-zone transient storage modeling using temperature and solute data with multiobjective calibration: 2. temperature and solute. *Water Resources Research* **46**. doi:10.1029/2009WR008759.
- Null, SE, Ligare, ST, & Viers, JH, 2013. A method to consider whether dams mitigate climate change effects on stream temperatures. *Journal of the American Water Resources Association* **49**: 1456–1472. doi:10.1111/jawr.12102.
- Oke, T, 1987. *Boundary layer climates, second edition*. London: Routledge.
- Olden, JD & Naiman, RJ, 2010. Incorporating thermal regimes into environmental flows assessments: modifying dam operations to restore freshwater ecosystem integrity. *Freshwater Biology* **55**: 86–107. doi:10.1111/j.1365-2427.2009.02179.x.
- Parkinson, EA, Lea, EV, Nelitz, MA, Knudson, JM, & Moore, RD, 2016. Identifying temperature thresholds associated with fish community changes in British Columbia, Canada, to support identification of temperature sensitive streams. *River Research and Applications* **32**: 330–347. doi:10.1002/rra.2867.
- Penman, HL, 1956. Estimating evaporation. *Transactions, American Geophysical Union* **37**: 43–48. doi:10.1029/TR037i001p00043.
- Ploum, SW, Laudon, H, Peralta-Tapia, A, & Kuglerova, L, in press. Are hydrological pathways and variability in groundwater chemistry linked in the riparian boreal forest? *Hydrology and Earth System Sciences* pp. 1–16. doi:10.5194/hess-2019-339.
- R Core Team, 2019. *R: a language and environment for statistical computing*. R Foundation for Statistical Computing, Vienna, Austria.
- Richardson, JJ, Torgersen, CE, & Moskal, LM, 2019. Lidar-based approaches for estimating solar insolation in heavily forested streams. *Hydrology and Earth System Sciences* **23**: 2813–2822. doi:10.5194/hess-23-2813-2019.
- Schneider, CA, Rasband, WS, & Eliceiri, KW, 2012. Nih Image to ImageJ: 25 years of image analysis. *Nature Methods* **9**: 671–675. doi:10.1038/nmeth.2089.

- Sinokrot, BA & Stefan, HG, 1993. Stream temperature dynamics: measurements and modeling. *Water Resources Research* **29**: 2299–2312. doi:10.1029/93WR00540.
- Sridhar, V, Sansone, AL, LaMarche, J, Dubin, T, & Lettenmaier, DP, 2004. Prediction of stream temperature in forested watersheds. *Journal of the American Water Resources Association* **40**: 197–213. doi:10.1111/j.1752-1688.2004.tb01019.x.
- Sutton, OG, 1953. *Micrometeorology: a study of physical processes in the lowest layers of the earth's atmosphere*. McGraw-Hill, New York.
- Szeit, AJ, 2019. Predicting evaporation from mountain streams. Master's thesis, University of British Columbia. doi:10.14288/1.0380868.
- Vugts, HF, 1974. Calculation of temperature variations of small mountain streams. *Journal of Hydrology* **23**: 267–278. doi:10.1016/0022-1694(74)90007-9.
- Webb, BW & Zhang, Y, 1997. Spatial and seasonal variability in the components of the river heat budget. *Hydrological Processes* **11**: 79–101. doi:10.1002/(SICI)1099-1085(199701)11:1<79::AID-HYP404>3.0.CO;2-N.
- Weisman, RN & Brutsaert, W, 1973. Evaporation and cooling of a lake under unstable atmospheric conditions. *Water Resources Research* **9**: 1242–1257. doi:10.1029/WR009i005p01242.
- Westhoff, MC, Bogaard, TA, & Savenije, HHG, 2010. Quantifying the effect of in-stream rock clasts on the retardation of heat along a stream. *Advances in Water Resources* **33**: 1417–1425. doi:10.1016/j.advwatres.2010.02.006.
- Wichert, GA & Lin, P, 1996. A species tolerance index for maximum water temperature. *Water Quality Research Journal* **31**: 875–893. doi:10.2166/wqrj.1996.048.
- Yearsley, JR, 2009. A semi-Lagrangian water temperature model for advection-dominated river systems. *Water Resources Research* **45**. doi:10.1029/2008WR007629.
- Younus, M, Hondzo, M, & Engle, BA, 2000. Stream temperature dynamics in upland agricultural watersheds. *Journal of Environmental Engineering* **126**: 518–526.

Table 1: The base wind function (Model 0) and 11 expanded model forms incorporating canopy openness and stability variables. The models were fit to meteorological measurements made 0.5 and 1.5 m above the stream surface.

#	Model
0	$E = (a + b \cdot u) \cdot \Delta e$
1	$E = (a + b \cdot u + c \cdot \phi) \cdot \Delta e$
2	$E = (a + b \cdot u + c \cdot \gamma) \cdot \Delta e$
3	$E = (a + b \cdot u + c \cdot \phi \cdot u) \cdot \Delta e$
4	$E = (a + b \cdot u + c \cdot \gamma \cdot u) \cdot \Delta e$
5	$E = (a + b \cdot u + c \cdot \phi + d \cdot \gamma) \cdot \Delta e$
6	$E = (a + b \cdot u + c \cdot \phi \cdot u + d \cdot \gamma) \cdot \Delta e$
7	$E = (a + b \cdot u + c \cdot \phi + d \cdot \gamma \cdot u) \cdot \Delta e$
8	$E = (a + b \cdot u + c \cdot \phi \cdot u + d \cdot \gamma \cdot u) \cdot \Delta e$
9	$E = (a + b \cdot \phi \cdot u) \cdot \Delta e$
10	$E = (a + b \cdot \phi \cdot u + c \cdot \gamma) \cdot \Delta e$
11	$E = (a + b \cdot \phi \cdot u + c \cdot \gamma \cdot u) \cdot \Delta e$

Table 2: Stream physiography, average wind speeds, and differences in wind speed. The sheltering ratio is computed as tree height  $\div$  stream width, and  $u_h$  refers to wind speed in  $\text{m s}^{-1}$  measured  $h$  metres above the stream surface. The streams are arranged by decreasing values of wind speed difference.

Stream	Canopy Open- ness	Sheltering Ratio	$u_{1.5}$	$u_{0.5}$	$\Delta u$
Blaney Ck. (Lower)	0.09	8.41	0.61	0.39	0.22
Blaney Ck. (Upper)	0.24	4.21	0.30	0.16	0.14
Spring Ck.	0.16	10.55	0.38	0.26	0.12
Rutherford Ck.	0.70	0.29	1.63	1.53	0.10
Marion Ck.	0.11	7.88	0.45	0.38	0.07
Miller Ck.	0.57	0.97	0.48	0.42	0.05
Alouette R.	0.45	1.83	1.27	1.25	0.02
Cayoosh Ck.	0.50	0.86	1.19	1.17	0.02
North Alouette R.	0.15	4.19	0.17	0.18	-0.01

Table 3: A comparison of wind function coefficients,  $a$  and  $b$ , derived from stream evaporation measurements, and two commonly cited in stream temperature modelling studies. In the seventh column,  $T_p$  indicates the evaporation pan water temperature. The units of  $a$  and  $b$  are  $\text{mm h}^{-1} \text{kPa}^{-1}$  and  $\text{mm h}^{-1} \text{s m}^{-1} \text{kPa}^{-1}$ , respectively.

Source	Site Description	Wind Function ( $a + b \cdot u$ )	Measurement height (m)	Stream width (m)	$T_p$ measured?
This study ( $e_{w,pan}$ )	Forested streams	$0.0663 + 0.0449 \cdot u$	1.5	3.1 to 27.6	yes
		$0.0815 + 0.0437 \cdot u$	0.5		
This study ( $e_{w,stream}$ )	Forested streams	$0.0699 + 0.0549 \cdot u$	1.5	3.1 to 27.6	yes
		$0.0699 + 0.0661 \cdot u$	0.5		
Benner (2000)	Streams in meadows and forest	$0.144 + 0.085 \cdot u$	0.5	2.7 to 19.5	yes
Guenther et al. (2012)	Forested stream	$0.0424 \cdot u$	1.5	1.5	yes
Maheu <i>et al.</i> (2014)	Forested stream	$0.11 + 0.122 \cdot u$	2	8	no
	Forested stream	$0.123 + 0.035 \cdot u$	2	80	no
	Forested stream	$0.047^n + 0.074^n \cdot u$	2	80	no
Caissie et al. (2016)	Forested stream	$0.19 \cdot u$	2	1.7	no
Brady et al. (1969)	Powerplant cooling lake	$0.101 + 0.005^* \cdot u^2$	7	-	-
Webb and Zhang (1997)	Streams in pasture and woodland	$0.055 + 0.059 \cdot u$	2	-	-

<sup>n</sup> wind function coefficients derived from night-time measurements

\* coefficient units of  $\text{mm h}^{-1} \text{s}^2 \text{m}^{-2} \text{kPa}^{-1}$

Table 4: Goodness-of-fit statistics computed from leave-one-out cross-validated model predictions for a selection of models. The root-mean-square error (RMSE,  $\text{mm h}^{-1}$ ) and the Nash-Sutcliffe efficiency (NSE) are the model goodness-of-fit statistics provided.

	#	Model	RMSE	NSE
1.5 m	0	$E = (a + b \cdot u) \cdot \Delta e$	0.0187	0.862
	11	$E = (a + b \cdot \phi \cdot u + c \cdot \gamma \cdot u) \cdot \Delta e$	0.0166	0.891
0.5 m	0	$E = (a + b \cdot u) \cdot \Delta e$	0.0162	0.897
	9	$E = (a + b \cdot \phi \cdot u) \cdot \Delta e$	0.0159	0.900

Table 5: The population-level estimated coefficients and coefficient standard errors for the selected models.

		Estimated coefficient value [standard error]		
	#	$a$ (mm h <sup>-1</sup> kPa <sup>-1</sup> )	$b$ (mm h <sup>-1</sup> s m <sup>-1</sup> kPa <sup>-1</sup> )	$c$ (mm h <sup>-1</sup> s <sup>3</sup> m <sup>-2</sup> kPa <sup>-1</sup> )
1.5 m	0	0.0663 [0.0079]	0.0449 [0.0069]	-
	11	0.0837 [0.0033]	0.1201 [0.0169]	0.0766 [0.0234]
0.5 m	0	0.0815 [0.0049]	0.0437 [0.0072]	-
	9	0.0944 [0.0034]	0.0684 [0.0069]	-

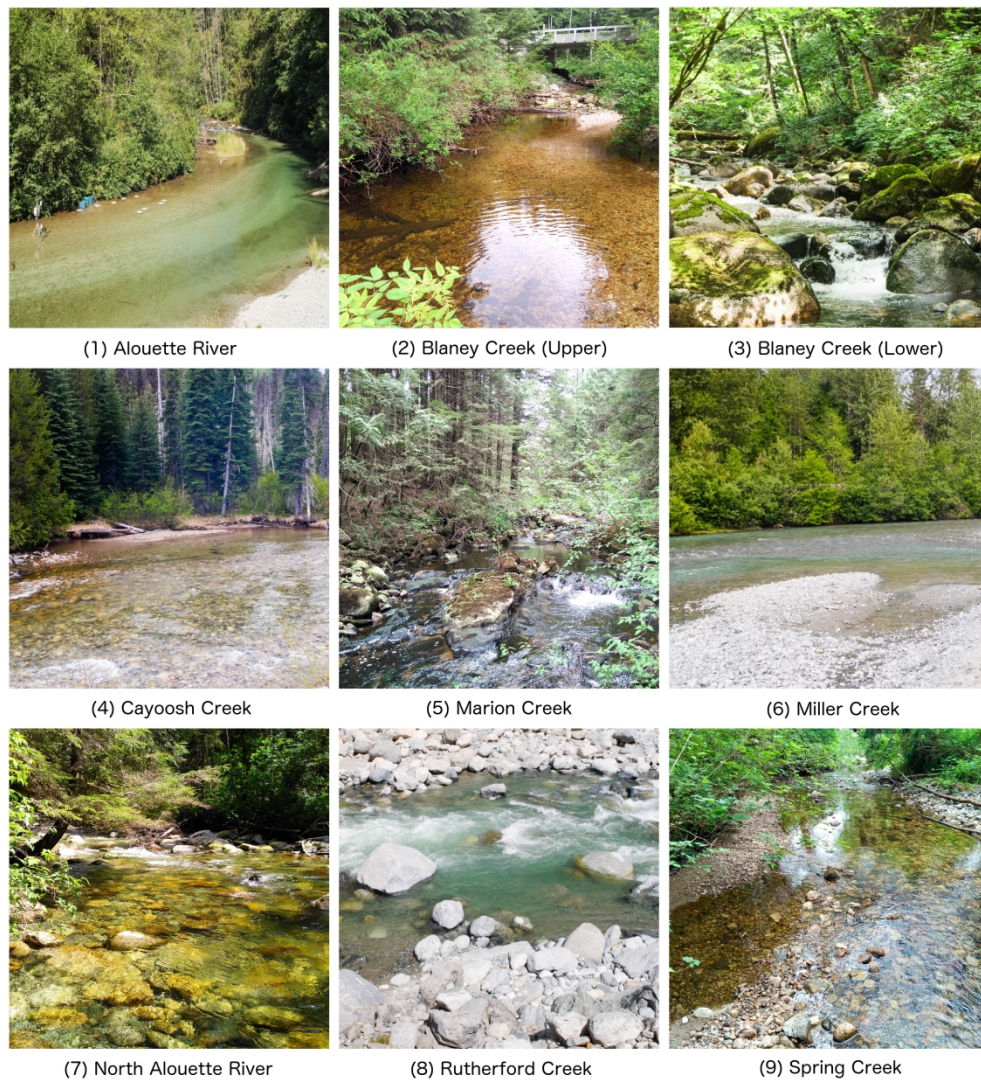


Figure 1: Photographs of the nine study sites.

199x218mm (300 x 300 DPI)

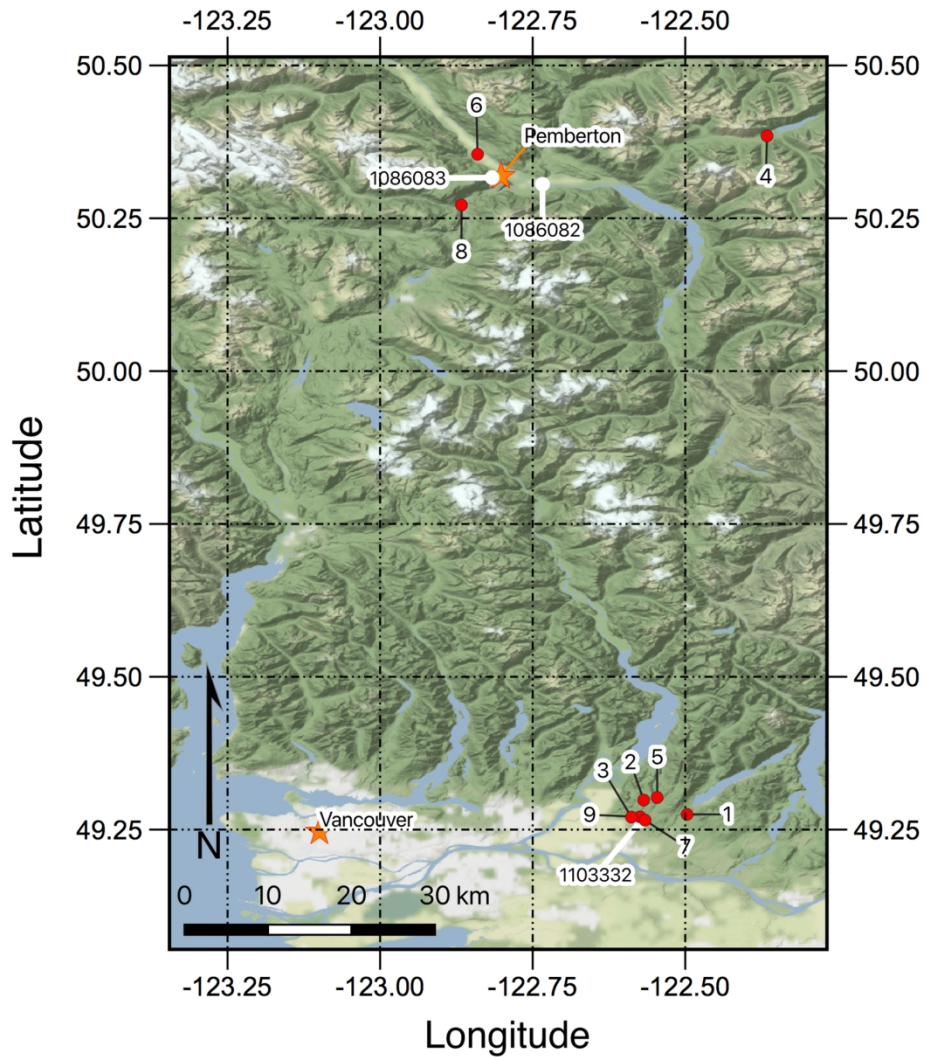


Figure 2: The locations of the study streams, indicated by red dots, in southwest British Columbia. The climate stations providing data of the regional hydroclimate are indicated by white dots and labelled with their Environment and Climate Change Canada climate station ID. Figure 1 provides the stream names that correspond to the stream numbers. The inland streams are numbered 4, 6, and 8, and the remaining streams are the coastal streams. The base map source is the Stamen Terrain tile set © OpenStreetMap contributors.

462x524mm (600 x 600 DPI)

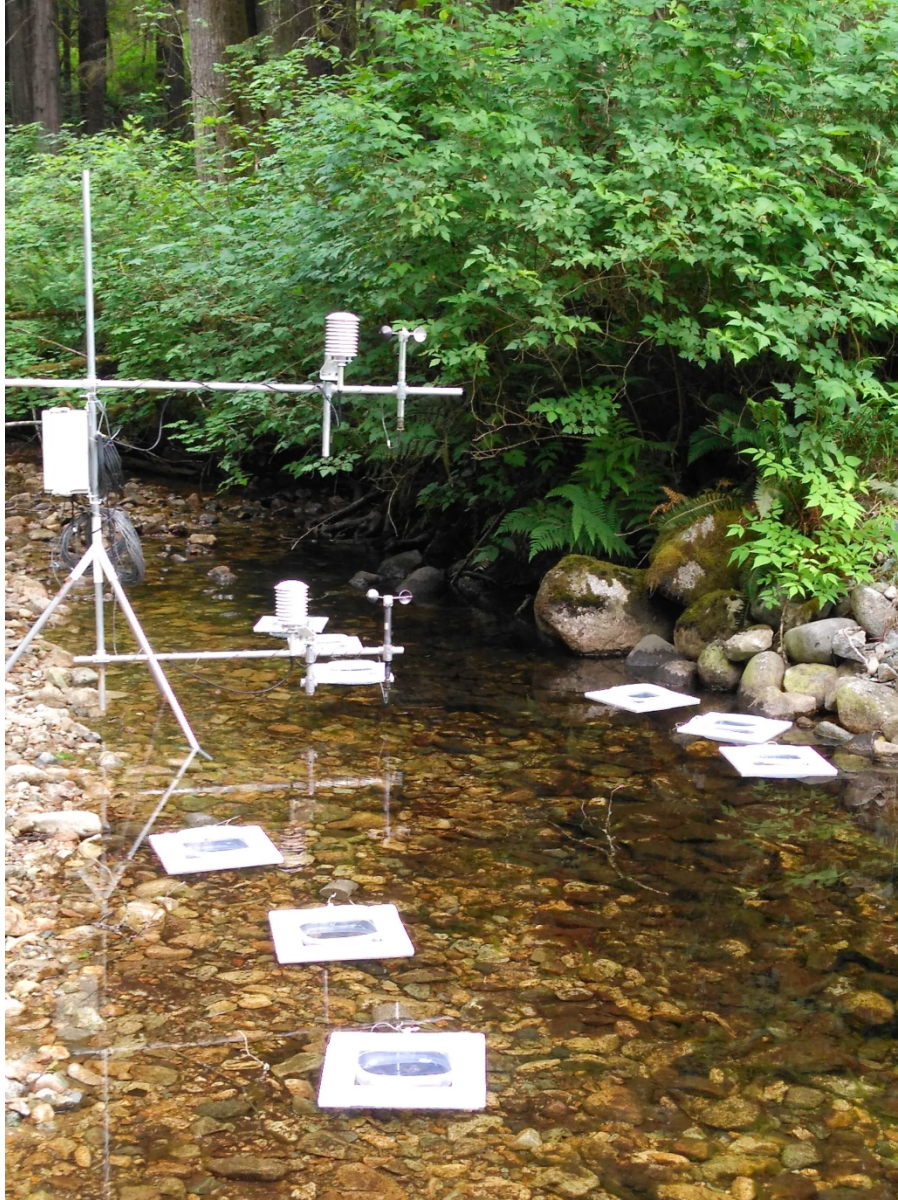


Figure 3: The evaporation pans and meteorological station set up at Spring Creek. The TidbiT water temperature logger is submersed near the meteorological station. This demonstrates the ideal distribution of evaporation pans in a stream and the location of the meteorological station with respect to the pans; individual stream characteristics resulted in deviations from this ideal.

103x138mm (600 x 600 DPI)

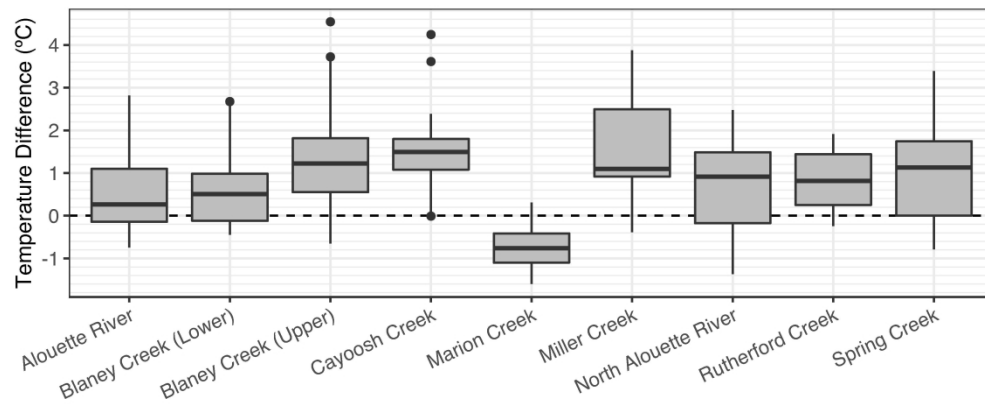


Figure 4: The stream-averaged distributions of water temperature difference between the evaporation pans and the stream.

179x79mm (600 x 600 DPI)

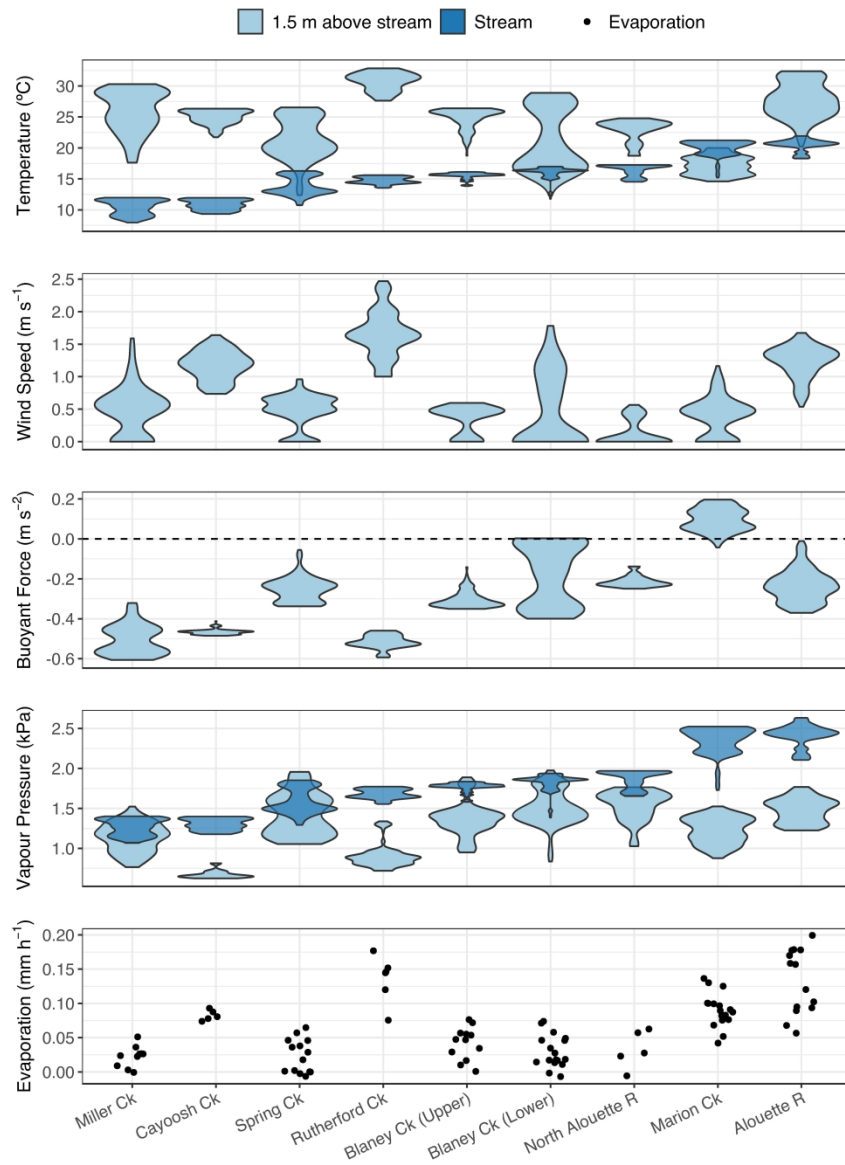


Figure 5: The distributions of meteorological conditions at each stream during stream evaporation measurements, arranged by increasing mean stream temperature.

199x279mm (600 x 600 DPI)

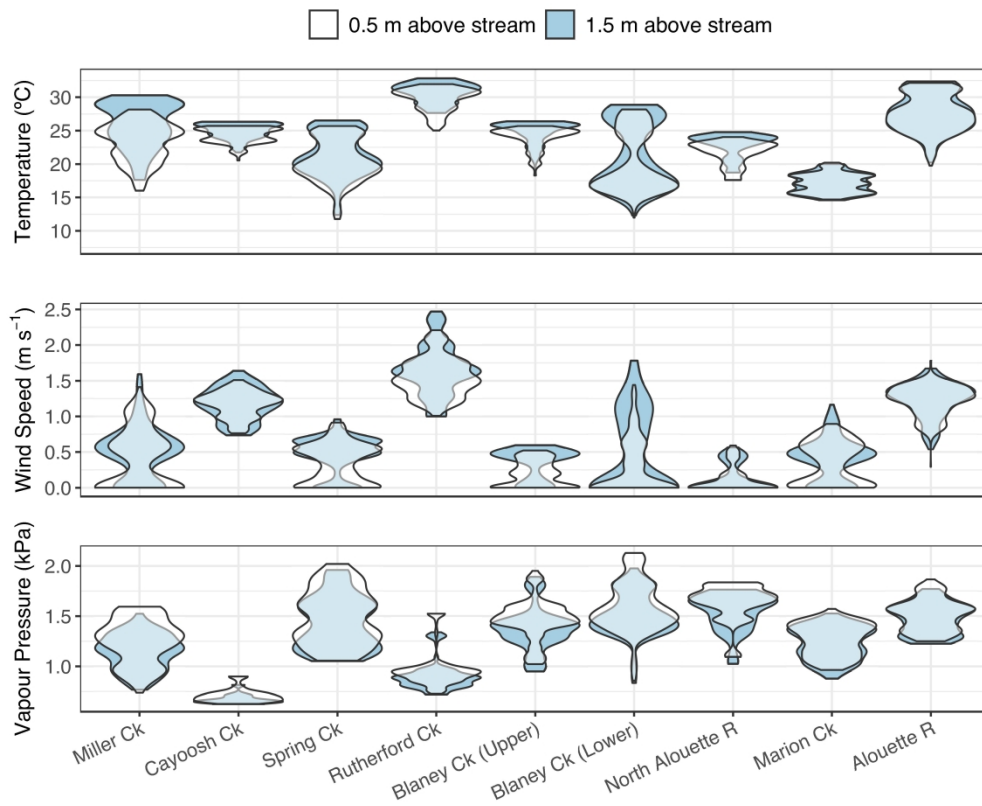


Figure 6: The distributions of meteorological conditions measured 0.5 and 1.5 m above the stream surface, arranged by increasing mean stream temperature.

199x169mm (600 x 600 DPI)

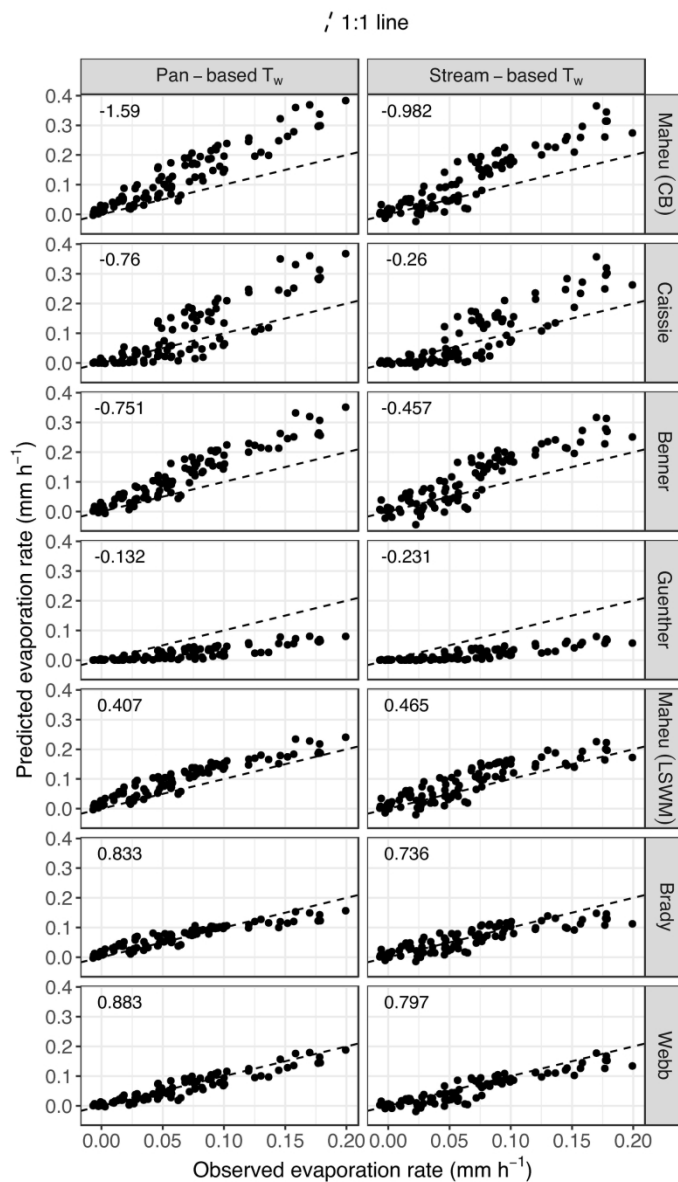


Figure 7: Comparison of the evaporation rates estimated by applying seven literature wind functions to this study's dataset. The wind function coefficients and the study references are provided in Table 3. The two panels for Maheu correspond to the wind functions for Catamaran Brook (CB) and the Little Southwest Miramichi River (LSWM). The panels are ordered from 1 to 7 by decreasing model root-mean-square error, and the Nash-Sutcliffe efficiency is provided in the top-left corner of each panel.

149x260mm (300 x 300 DPI)

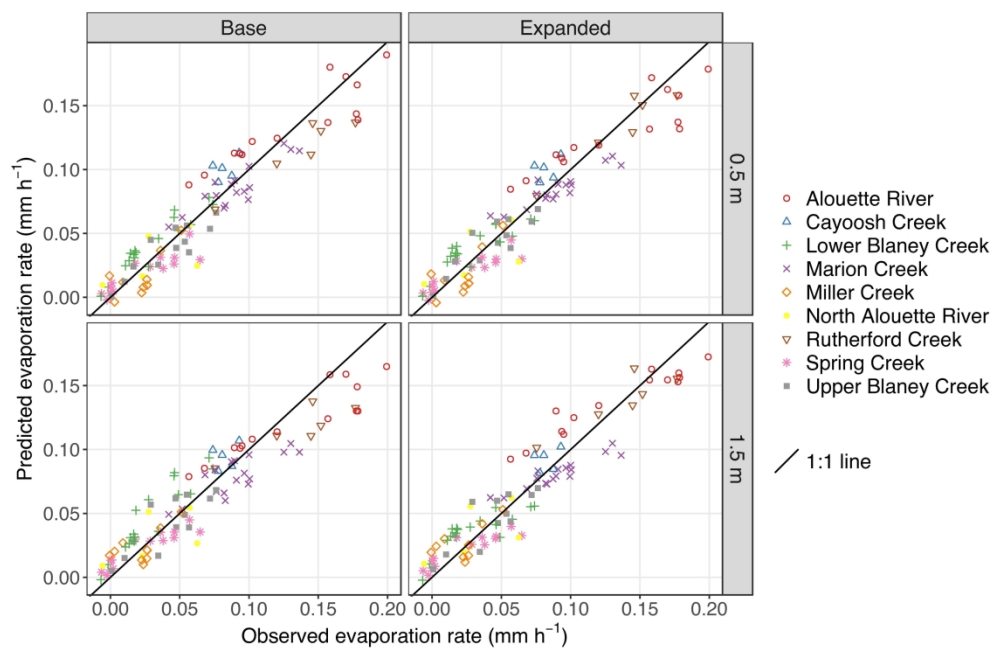


Figure 8: Cross-validated model predictions for the base mass transfer model and the two best expanded models, Models 9 and 11, for meteorological measurements made 0.5 m and 1.5 m above the stream surface, respectively.

260x169mm (300 x 300 DPI)

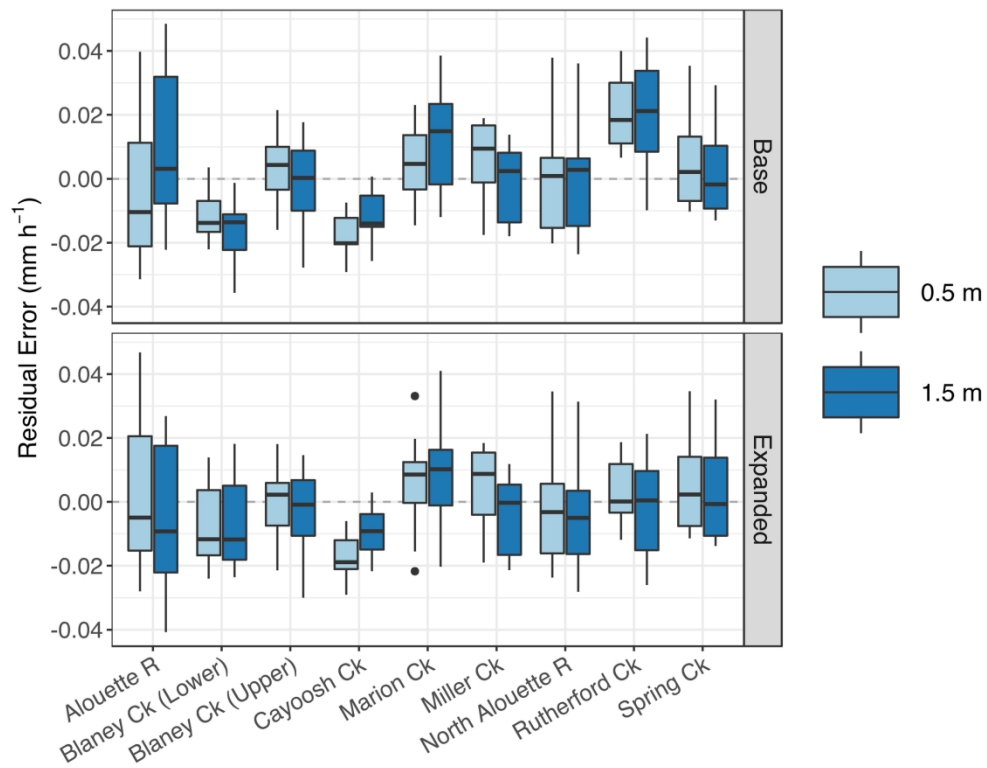


Figure 9: The site-specific residual error distribution for the base and expanded 0.5-m and 1.5-m models. The residuals were computed from cross-validated model predictions.

199x159mm (300 x 300 DPI)